THE JOURNAL OF PHYSICAL CHEMISTRY B

Article

Cite This: J. Phys. Chem. B 2019, 123, 3024−3032

pubs.acs.org/JPCB

Structural Origins of RF_3/$NaRF_4$ Nanocrystal Precipitation from Phase-Separated $SiO_2-Al_2O_3-RF_3-NaF$ Glasses: A Molecular Dynamics Simulation Study

Junjie Zhao,[†,‡] Xiuxia Xu,[†,‡] Pengcheng Li,[†] Xinyue Li,[§] Daqin Chen,[∥] Xvsheng Qiao,*[,†] Jincheng Du,*[,‡] Guodong Qian,[†] and Xianping Fan[†]

[†]State Key Laboratory of Silicon Materials & School of Materials Science and Engineering, Zhejiang University, Hangzhou 310027, China

[‡]Department of Materials Science and Engineering, University of North Texas, Denton, Texas 76203, United States

[§]College of Materials and Environmental Engineering, HangZhou Dianzi University, Hangzhou 310018, China

[∥]College of Physics and Energy, Fujian Normal University, Fuzhou 350117, China

Supporting Information

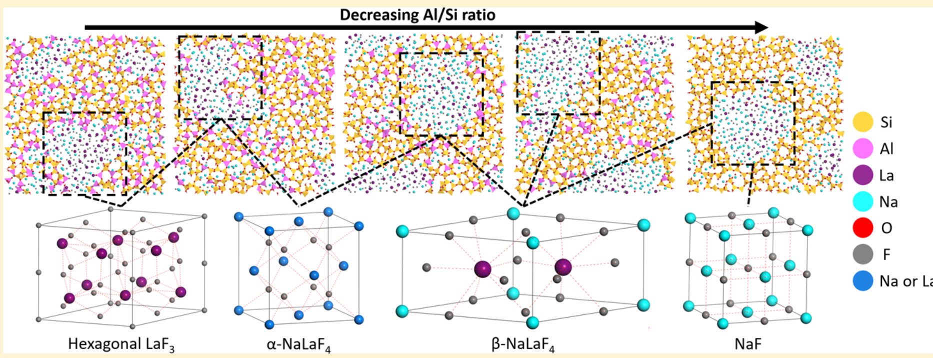

ABSTRACT: Oxyfluoride glass-ceramics with RF_3 or $NaRF_4$ (R^{3+}: rare earth elements) nanocrystals are considered as favorable hosts for luminescence applications. In this work, we utilized large-scale molecular dynamics (MD) simulations with effective partial charge potentials to study a series of oxyfluoride glasses that are of interest to the precipitation of RF_3 or $NaRF_4$ nanocrystals as previous experiment results suggested. The results show that phase separation exists in all glass compositions with fluoride-rich regions made up of R^{3+}, Na^+, and F^- and oxide-rich regions consisting of aluminosilicate networks. These fluoride-enriched regions can serve as the precursor for RF_3, cubic and hexagonal $NaRF_4$, and NaF crystal precipitation. The results also confirm that the concentration of Na^+ in the fluoride phase plays a key role in determining the crystal phases (RF_3, $NaRF_4$, or NaF) and crystal structure (cubic vs hexagonal $NaRF_4$) to be precipitated. Consequently, this study shows that MD simulations with effective potentials can fill the gap in the structural understanding of oxyfluoride glass and provide insights into atomic scale information of the phase separation behavior that is useful in predicting the potential crystal types in oxyfluoride glass. When coupled with experimental validations, these simulations can expedite the exploration of novel luminescent oxyfluoride glass ceramics.

Downloaded via COLUMBIA UNIV on October 22, 2019 at 10:14:43 (UTC).
See https://pubs.acs.org/sharingguidelines for options on how to legitimately share published articles.

1. INTRODUCTION

Oxyfluoride glass-ceramics with fluoride nanocrystals imbedded in the oxide glass matrix are promising hosts for lanthanide (or rare earth) ions containing luminescence systems.[1] The fluoride nanocrystals have lower phonon energy[2] and higher solubility for lanthanide ions[3] while the oxide matrix can stabilize the fluoride nanocrystals and provide excellent mechanical properties and chemical durability.[4] These advantages make oxyfluoride glass ceramics excellent candidates for photonic applications such as spectral converters,[5] solid-state lightings,[6,7] laser hosts,[8,9] fibers,[10] and optical temperature sensors.[11,12]

Among various fluoride nanocrystals, rare-earth fluorides, RF_3 (R = Y^{3+}, La^{3+}, Gd^{3+}, Yb^{3+}, etc.), and sodium rare-earth fluorides, $NaRF_4$, are considered as ideal hosts for lanthanide (Ln^{3+}) ion upconversion luminescent activators. The RF_3 and $NaRF_4$ crystals provide small lattice mismatch for other Ln^{3+} ionic activators because of their similar chemical behaviors and ionic radii. It is because of these additional benefits, oxyfluoride glass ceramics that are capable to precipitate RF_3 or $NaRF_4$ nanocrystal phases have been intensively studied for more than

Received: February 20, 2019
Revised: March 13, 2019
Published: March 13, 2019

ACS Publications © 2019 American Chemical Society

20 years.[13] Muñoz et al.[14] suggested that the crystallization competition between RF_3 and $NaRF_4$ phases in fluoride-containing aluminosilicate glasses may be because of the abundance of Al−F−Na and R−F linkages. After thermal treatment, the fluorine ions in Al−F−Na linkages in the glass matrix will diffuse into the fluoride-rich regions, leading to enhancement of phase separation. As a result, fluorine ions preferentially coordinate with R^{3+} in the fluoride phase, being one of the reasons for the favorable RF_3 precipitation.[15] On the other hand, studies[16−18] suggested that higher SiO_2 and lower Al_2O_3 concentration favor the precipitation of $NaRF_4$ than RF_3 phases. The exact structural origin of this selective crystal precipitation, however, is far from being fully understood.

In particular, how to obtain transparent glass-ceramics with hexagonal $NaRF_4$ nanocrystals has been extensively discussed. The upconversion efficiency of Ln^{3+} ions in the hexagonal phase is at least one order of magnitude higher than that in the cubic one[19,20] because of the anisotropy nature[21] and the favorable coordination environment for dopants in the hexagonal phase.[22,23] It was found that the preferential hexagonal $NaRF_4$ crystalline structure not only relies on the thermal process conditions[24−26] but also on the internal pressure[27] and the glass composition, such as Al/Si[8,20] or Na/R[28] ratios. Therefore, designing glass composition to obtain the aimed crystalline phase is one of the feasible ways in preparing oxyfluoride glass-ceramics with satisfying luminescent properties.

Despite many experimental efforts to form these glass ceramics with certain targeted fluoride crystalline phases, the understanding of crystallization process and selective precipitation of certain crystal phases are largely empirical and rely on trial-error approaches. One of the main reasons for this is because of the lack of understanding for the atomic structures and phase separation behaviors that are critical for the crystal formation in these mixed anion glasses. It has been widely accepted that fluoride phase separation is the initial stage of crystallization in oxyfluoride glass[29,30] with extensive experimental evidences of CaF_2,[31] SrF_2,[32] BaF_2,[33] LnF_3,[15,18,34] and $NaLnF_4$[24,35,36] precipitations from phase-separated regions. Thus, understanding how the change of glass compositions affects the fluoride phase separation and the remaining silicate-rich phase is a key in designing oxyfluoride glass-ceramics. However, owing to the amorphous nature of glass materials, it is hard to fully understand the glass structure by experimental approaches alone.

Our previous works[37,38] show that molecular dynamics (MD) simulation is a valuable theoretical method to understand the glass chemistry characteristics and the structural features in fluoride phase separation in aluminosilicate glass. MD simulation has been proved to be an efficient method to understand the glass structure and structure−property relations from atomic level.[39] Recently, with the development of empirical potentials, glass systems with multiple anions (such as O/F,[38,40] O/Cl[41,42]) have been studied and the results are found to be in favorable comparison with the experiments. In our earlier study,[37] phase separation into the oxide-rich phase consisting $[SiO_4]$ and $[AlO_4]$ formers and in the fluoride-rich phase with modifier enriching was observed with the help of MD simulations.[43,44] The compositions in fluoride-rich regions are in good agreement with those in the precipitated crystal phases observed in experiments. Hence, our hypothesis is that by the composition in the fluoride-rich phase obtained from MD simulations, we can predict the types of precipitated fluoride nanocrystals in oxyfluoride glass-ceramics.

In this study, by using MD simulations with effective partial charge potentials, we aim to understand the structure origins of RF_3 and $NaRF_4$ nanocrystal precipitation and the compositional-dependent phase selection between the cubic and hexagonal $NaRF_4$ crystalline phases from the fluoride-rich regions in the aluminosilicate glass matrix. Here, we take La^{3+} as the representative of all the R^{3+} ions,[8] partly because of the chemistry similarity among rare-earth ions and partly because of the availability of potential parameters. By varying the Al/Si ratio, we have studied a series of compositions in the SiO_2−Al_2O_3−Na_2O−NaF−LaF_3 system. The compositions were chosen so that experimental crystallization results[45] are available for comparison. In particular, experimental results[45] suggest that crystal precipitations are in the sequence of LaF_3, cubic $NaLaF_4$, hexagonal $NaLaF_4$, and NaF phases with lowering Al/Si ratio. After melting and quenching processes to form the glass samples, visualization method and short- and medium-range structural analysis were utilized to describe both silicate phase and fluoride phase in selected aluminosilicate oxyfluoride glass. The atomic structure features and the compositional effects on fluoride phase separation were also studied. By combining the MD simulation results and comparison with previous experimental results, this work proves that MD simulation can provide valuable insightful information interpreting experimental phenomena and eventually help to explore possible crystalline phases in oxyfluoride glass-ceramics through composition design.

2. COMPUTATIONAL DETAILS

Based on the previous experimental study[8,45] that showed the change of the Al/Si ratio affecting the precipitation crystal phases, we chose glass compositions with fixed Na_2O, NaF, and LaF_3 contents but varying Al_2O_3 to SiO_2 ratios in the series of $(64 - x)SiO_2$−xAl_2O_3−19NaF−10Na_2O−8LaF_3 (mol %), x = 12, 9, 6, 3, and 0. These glass samples were studied using MD simulations with the DL_POLY 2.20 package[46] and named by GxAl where x represents the mole percent of alumina indicated in the formula above. Around 15 000 atoms were used in the simulation cells in order to properly represent statistical changes in the structures of the fluoride-rich regions and silicate-rich regions after phase separation. The number of atoms used in the simulation and the Al/Si ratio are listed in Table 1.

Table 1. Amount of Each Atoms and Al/Si Ratio for Each Simulation Cell

sample name	Si	Al	Na	La	O	F	Al/Si
G12Al	2600	1200	1950	400	7500	2150	0.23
G9Al	2750	900	1950	400	7350	2150	0.16
G6Al	2900	600	1950	400	7200	2150	0.10
G3Al	3050	300	1950	400	7050	2150	0.05
G0Al	3200	0	1950	400	6900	2150	0.00

In this study, we used the modified Teter potential[43,44] expanded by Du et al., which has been widely used in silicate,[47,48] aluminosilicate,[49,50] phosphate,[51] and recently, based on new potential development, borosilicate[52,53] glasses. This set of partial charge potential has also been shown to be capable to model oxyfluoride mixed anion glasses.[38,40] For each glass composition, three parallel samples were prepared for

DOI: 10.1021/acs.jpcb.9b01674
J. Phys. Chem. B 2019, 123, 3024−3032

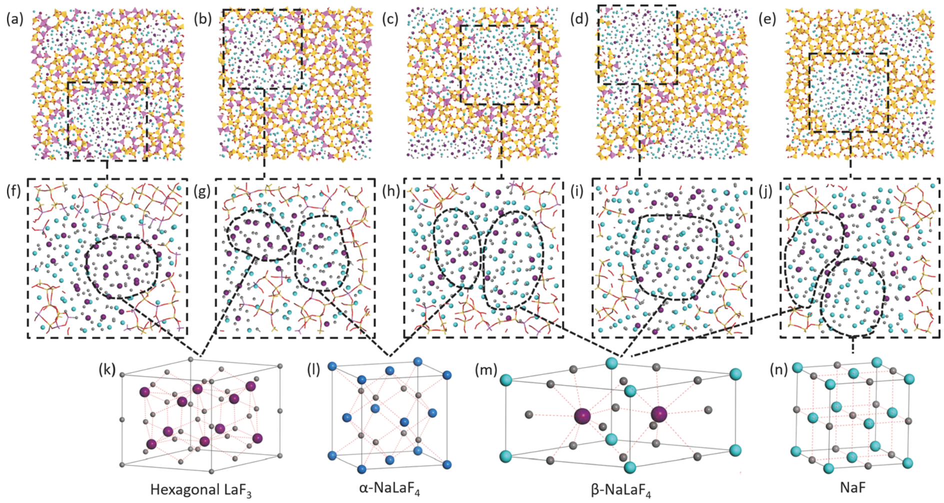

Figure 1. Snapshots from the final configuration of G12Al (a), G9Al (b), G6Al (c), G3Al (d), and G0Al (e) after equilibrium at 300 K. The length of each simulation bulk is around 59 Å and the snapshots show the cross-section for about two layers of atoms in thickness. (f−j) Magnifications for the separated fluoride phase from the above samples, respectively. Crystalline phases of LaF_3 (k), cubic $NaLaF_4$ (l), hexagonal $NaLaF_4$ (m), and NaF (n) can precipitate from the corresponding fluoride phase.[45] Yellow: Si, pink: Al, purple: La, cyan: Na, grey: F, and red: O. The blue ball in (l) indicates that Na^+ and La^{3+} can randomly occupy these cation sites in cubic $NaLaF_4$.[21]

each sample with different initial random structures and the statistics analysis was averaged among the three samples.

During the simulation, the simulated melt and quench procedure was applied to generate the glass structures. After generating the initial structure with atoms being randomly distributed in the simulation cell, the glass samples were first heated to 6000 K to fully melt the system. The cooling went through a two-stage process with a step-wise cooling procedure. The first stage cooling is from 6000 to 1500 K, with a cooling rate of 5.6 K/ps. The simulation ensembles used in this stage are constant volume ensembles: canonical (nVT) followed by microcanonical (nVE) at each temperature stair. The second stage cooling from 1500 to 300 K used a cooling rate of 1.1 K/ps with constant temperature and pressure (nPT) and followed the nVE ensemble at each temperature. The final simulation trajectories for structural analysis with 800 frames in total are recorded every 0.05 ps at 300 K. The reasons to choose this cooling procedure are to ensure full equilibration of the melts at high temperatures and to avoid abnormal volume expansion at high temperatures while allowing the glasses to equilibrate under ambient pressure at lower temperatures.

The Materials Studio software was used to visualize the final glass structures and perform initial structural analysis. Short and medium range structure analyses were performed with the trajectory recorded at the final stage of the simulations. For the short-range structure, bond angle distribution (BAD) and coordination number (CN) were analyzed. BAD describes the distribution of the angles formed by a center atom with two adjacent atoms. The intensity of BAD can be referred as an indication for the coordination preference in certain environment. CN is the number of atoms in the coordination shell of one center atom.

The change of the medium-range structure (4−10 Å) is also important for the glass properties because glass is a material that has an ordered short-range structure (0−4 Å) but lacks the long-range structure (>10 Å). For the medium-range structure, we mainly focus on the Q_n distribution, network connectivity, and ring size distribution. Q_n means the number (n) of bridging oxygen (BO) coordinating with one glass network former atom (Q). BO is the oxygen coordinating with two network former atoms while non-BO (NBO) stands for the oxygen atom bonding with one glass former and one glass modifier. By examining the Q_n of each glass former species, Si^{4+} and Al^{3+} in this study, we can know how the change of the Al/Si ratio affects the oxide phase structure. The network connectivity is calculated based on the Q_n of each glass former with the power of its amounts.[52] In addition, the ring size distribution can help to examine the stability of the oxide phase against the composition change, which is important for the controllable crystallization and glass composition design.

During the analyses of glass structures, it is necessary to define bonding between atom pairs where a cutoff distance is used. The cutoff distance for atom pairs in the above structural analysis is from the first minimum from the partial pair distribution function (PDF). The PDF, cation−anion bond distance, and the cutoff values are provided in the Supporting Information.

3. RESULTS

3.1. Fluoride-Phase Separation in the Aluminosilicate Glass. All of the five samples (Figure 1a−e) show the fluoride-phase separation behavior with F^-, Na^+, and La^{3+} separating from the aluminosilicate oxide matrix. Based on our structural model proposed from the previous paper,[37] this phase separation phenomenon can be explained by the immiscibility nature of the fluoride and oxide networks. The oxide phase has similar structure features as the aluminosilicate oxide glass constructed by $[SiO_4]$ and $[AlO_4]$, with Na^+ randomly distributing throughout the oxide network, which can be described by Greaves's modified random network model.[54] In contrast, the structure of the fluoride-rich phase is similar to that in the fluoride glass made up by $[LaF_x]$ and $[NaF_x]$ polyhedral, which was explained by Poulain's ionic model.[55] Specially, the oxide-fluoride phase interface is mainly built up by cations in the mixed coordination environment, such as $[LaO_xF_y]$ and $[NaO_xF_y]$ polyhedral and $[AlO_xF_y]$ tetrahedra, maintaining the stability of glass samples.

DOI: 10.1021/acs.jpcb.9b01674
J. Phys. Chem. B 2019, 123, 3024−3032

With less introduction of Al_2O_3 in the glass compositions (lower Al/Si ratio), more Na^+ ions were found in the fluoride phase and the size of the separated fluoride phase become bigger (Figure 1f–j). It is interesting to see that inside the fluoride phase of the sample G12Al and G9Al (Figure 1f, g), there is a region only containing La^{3+} and F^-, surrounded by a shell mainly consisting of Na^+ and F^-. This La–F-riched region can be considered as the initial stage of the LaF_3 crystallization. Similarly, in the sample G0Al, small regions only containing Na^+ and F^- can be found in the fluoride phase, where NaF crystals can precipitate. In the samples with intermediate amount of Al_2O_3 such as G6Al and G3Al, La^{3+} and Na^+ ions in the fluoride phase distribute more homogeneously as compared with the other three samples. These well-distributed Na–F–La regions can develop into $NaLaF_4$ crystals under certain treatment. Specifically, Na–F–La regions with different Na^+ concentration can initially develop into cubic or hexagonal $NaLaF_4$ nanocrystals as observed in the experiments. The precipitation of cubic $NaLaF_4$ relates to lower Na^+ concentration in the fluoride phase, while the hexagonal phase refers to be induced with higher Na^+ content. These composition variation and structural features of the fluoride-rich phases suggest that potential crystal phase formation is consistent with the experimentally observed sequence of crystal phases as a function of Al/Si ratios.[45]

Coordination number (CN) (Figure 2a,b) also shows Na^+ preferentially enrich in the fluoride phase while the coordination environment of La^{3+} still dominated by fluorine with the decreasing Al/Si ratio. The average Na^+ CN is slightly larger than 6 while the average La^{3+} CN is around 8.5. Both oxygen and fluorine exist in the coordination shell of these two cations but La^{3+} has a higher fraction of fluorine coordination than oxygen. The coordination environment of La^{3+} is stable against the drop of the Al/Si ratio, only with slight decrease in La–O CN lead by the reduction in the La–BO type. On the other hand, the coordination environment of Na^+ change dramatically compared to La^{3+}'s. With Al_2O_3 being substituted by SiO_4, in the oxide phase, the number of BO bonds with Na^+ drop, leading to the decrease of CN. The drop of the BOs relates to the decrease of Al^{3+}, which require charge compensators, Na^+ in this study, to maintain neutrality. With the Al/Si ratio less than 0.05, more fluorine than oxygen enters into Na^+'s coordination environment, confirming the enrichment of Na^+ in the fluoride phase in visualize observation (Figure 1).

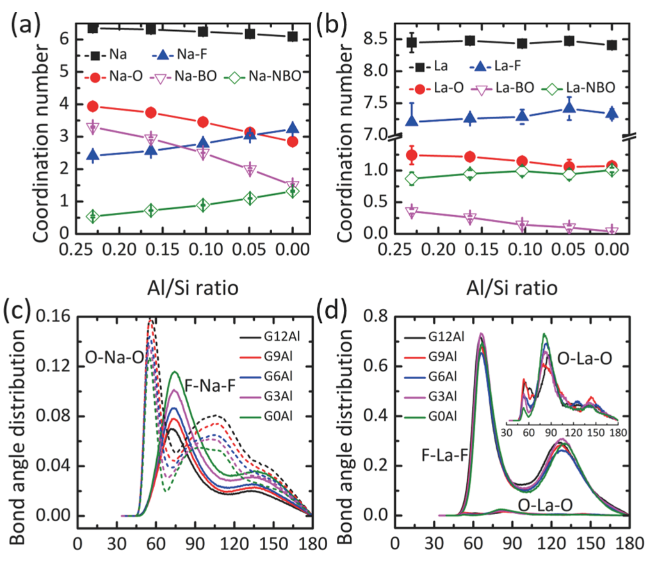

Figure 2. CN of Na^+ (a) and La^{3+} (b). BAD of Na^+ (c) and La^{3+} (d) in oxide (O–M–O) and fluoride (F–M–F) environments.

In addition, Na^+'s preferential coordination into the fluoride phase under low Al^{3+} concentration is also confirmed by BAD (Figure 2c,d). In the O–M–O (M = Na^+, La^{3+}) bonding type, the angle around 60° can be assigned to the modifier cation bond with O^{2-} in the same tetrahedron, while the angle at about 90° generally led by a modifier cation in the octahedral geometry connecting two O^{2-} belonging to different tetrahedral.[56] The intensity of both the peaks (around 60° and 90°) in O–Na–O drops while F–Na–F raises with less Al_2O_3, indicating fewer O–Na–O bondings in the aluminosilicate oxide phase and more Na^+ coordinate into the fluoride phase. Besides, the second peak in O–Na–O shifts from about 105° to 90°, showing that the oxide phase becomes slightly compacter with a lower Al/Si ratio.

3.2. Aluminosilicate-Rich Oxide Phase Structure Features.

No major change in the aluminosilicate-rich oxide matrix can be observed from the visualization method (Figure 3), which is good in terms of maintaining the glass stability when adjusting the glass composition. The number of Na^+ decreases while NBOs increase with the lowering Al/Si ratio, and in samples G3Al and G0Al, regions only consist with $[SiO_4]$ tetrahedra occur (Figure 3d,e: dot circles). The CNs (Figure 4a,b) of Si^{4+} and Al^{3+} confirm these changes in the visualization observation. The CN of Si^{4+} is 4 while that of Al^{3+} is slightly larger than 4, indicating the glass formers maintain the tetrahedra geometry. The Si^{4+} ions in this simulation are found to only bond to oxygen. Oxygen coordinating with Si^{4+} can be partitioned into BO, NBO, and for some compositions a small amount of three-bonded oxygen (TBO). TBOs were observed in aluminosilicate glasses in both simulation and experiments,[57,58] acting as a charge compensator.[59] With the decreasing Al/Si ratio, in the coordination shell of Si^{4+}, the BOs decrease slightly while the percentage of the NBOs rises accordingly. On the other hand, Al^{3+} can bond with both O^{2-}

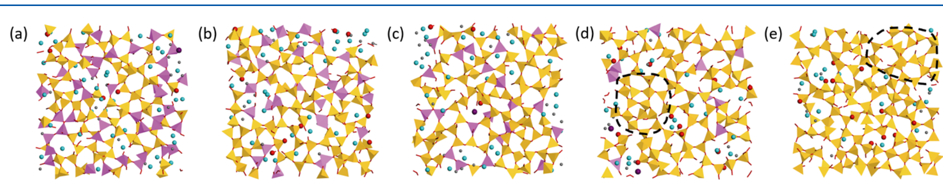

Figure 3. Snapshots of the magnified oxide phase of G12Al (a), G9Al (b), G6Al (c), G3Al (d), and G0Al (e). The size of each magnified oxide phase is around 30 Å in length and two layers of atoms in thickness. The dot circles emphasize that the regions only consist of $[SiO_4]$ tetrahedra. Yellow: Si, pink: Al, purple: La, cyan: Na, grey: F, and red: O. The red balls in each sample represent the NBOs.

DOI: 10.1021/acs.jpcb.9b01674
J. Phys. Chem. B 2019, 123, 3024–3032

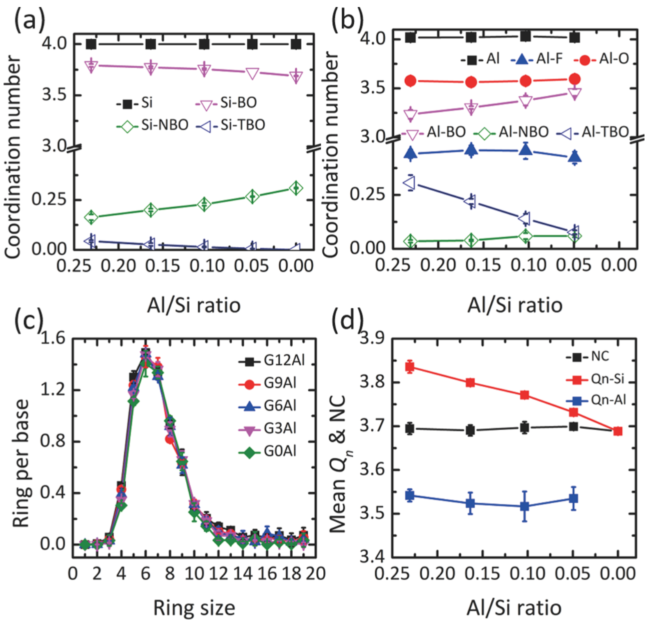

Figure 4. CN of Si^{4+} (a) and Al^{3+} (b), ring size distribution with the ring formed by $[SiO_4]$ and $[AlO_4]$ tetrahedra (c), and Q_n of Si^{4+} and Al^{3+} and the calculated network connectivity (d).

and F^-. The average CN of Al−F is below 0.5, indicating that most of Al^{3+} only coordinate with at most 1 F^-. With a lower Al/Si ratio, the BOs and NBOs increase while the TBOs decrease in Al^{3+}'s coordination shell. With less Al^{3+} and enough Na^+ in the network, charge compensator TBO is not preferred, and therefore its number drops and leads to the increase of Al−BO with the decreasing Al/Si ratio.

The medium range structures, as represented by the ring size distribution in Figure 4c and average Q_n distribution or network connectivity in Figure 4d, do not have appreciable change with the Al/Si ratio in the glass series as well. The network connectivity fluctuates at around 3.7, with the average Q_n around Si^{4+} decreases and average Q_n around Al^{3+} increases slightly with the decreasing Al/Si ratio. With less Al^{3+}, Na^+ that stay in the oxide phase will coordinate with $[SiO_4]$, breaking the Si−O−Si bond and creating one NBO, leading to the drop of Q_n-Si. On the other hand, the decrease of the Al−F CN with the decreasing Al/Si ratio indicates that Al^{3+} tend to stay in the oxide network with lower Al_2O_3 concentration, neighboring with glass formers and giving to higher Q_n-Al. In addition, the ring size distribution shows little change with composition. The 6-membered rings dominate, which is common in most of the oxide glass system. Besides, 5-, 7-,and 8-membered rings are also the main species in the oxide network. As compared to the ring size distribution of sodium silicate glasses with different soda contents,[43] the observed ring size distribution suggests that although the glass compositions in this study have high modifier concentration, the aluminosilicate or silicate network remain highly connected. This suggests that glass modifiers have mostly enriched fluoride-separated phase, and hence supports the visual observation of phase separation in these glasses.

3.3. Interfacial Structure between the Aluminosilicate and Fluoride Phases.

In particular, the oxide-fluoride phase interface is important for the stability of the immiscible system. It can be recognized that the phase interface is built up by $[LaO_xF_y]$ and $[NaO_xF_y]$, linking with the oxide phase through $[SiO_4]$ and $[AlO_xF_y]$ tetrahedra (Figure 5f,g). When coordinating with $[SiO_4]$ from the oxide phase, glass modifiers coordinate with NBO (Figure 5f). When coordinating with $[AlO_xF_y]$ tetrahedra, the situations are more complicated. Glass modifiers on the phase interface can coordinate with $[AlO_xF_y]$ tetrahedra with terminal oxygen and/or fluorine (Figure 5g) as well as BO charge compensating $[AlO_xF_y]$ tetrahedra (Figure 5f).

In comparison to Figure 3, the number of NBOs on the two-phase interface is more than that in the aluminosilicate-rich oxide phase. With the decreasing Al/Si ratio, more $[SiO_4]$ with terminal oxygen (NBO) are on the two-phase interface (Figure 5a−e). This is different from our previous study[37] which suggested that the $[AlO_xF_y]$ species are the main part of the two-phase interface. This difference may be resulted from the addition of Na^+, which is easier to coordinate with $[SiO_4]$ and create NBO than Ba^{2+} used in previous study. Besides, the lower concentration of Al_2O_3 in this study (less than 12 mol %) is another reason. With fewer Al^{3+} in the network, the abundant glass modifiers have higher chance to coordinate with $[SiO_4]$ and create NBOs on the phase interface.

3.4. Na^+ Coordination as a Function of the Al/Si Ratio.

Figure 6 further explains the coordination state of glass modifier Na^+ in the oxide phase and the two-phase interface,

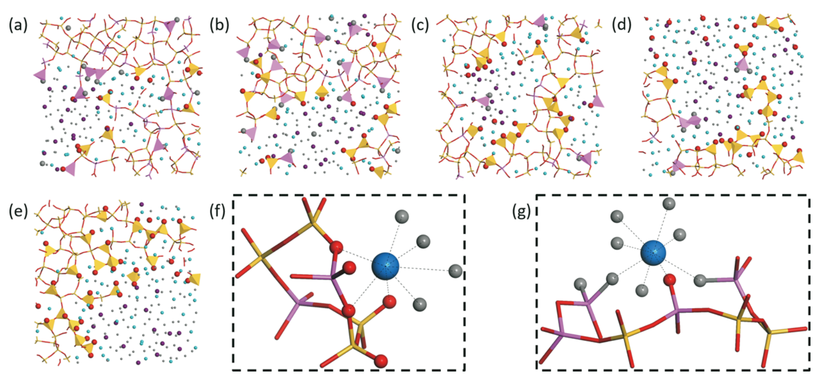

Figure 5. Snapshots of the oxide-fluoride phase interface in samples G12Al (a), G9Al (b), G6Al (c), G3Al (d), and G0Al (e). The size of each magnified phase interface is around 30 Å in length and two layers of atoms in thickness. (f) Local structure of $[MO_xF_y]$ (M = Na^+ or La^{3+}) coordinates with the oxide phase through NBO from $[SiO_4]$ and BO from $[AlO_4]$. (g) Local structure of $[MO_xF_y]$ (M = Na^+ or La^{3+}) coordinates with the oxide phase through nonbridging fluorine from $[AlO_xF_y]$ tetrahedra and NBO from $[AlO_4]$ tetrahedra. Yellow: Si, pink: Al, purple: La, cyan: Na, grey: F, and red: O. The blue balls in (f,g) indicate glass modifiers Na^+ and La^{3+}.

DOI: 10.1021/acs.jpcb.9b01674
J. Phys. Chem. B 2019, 123, 3024−3032

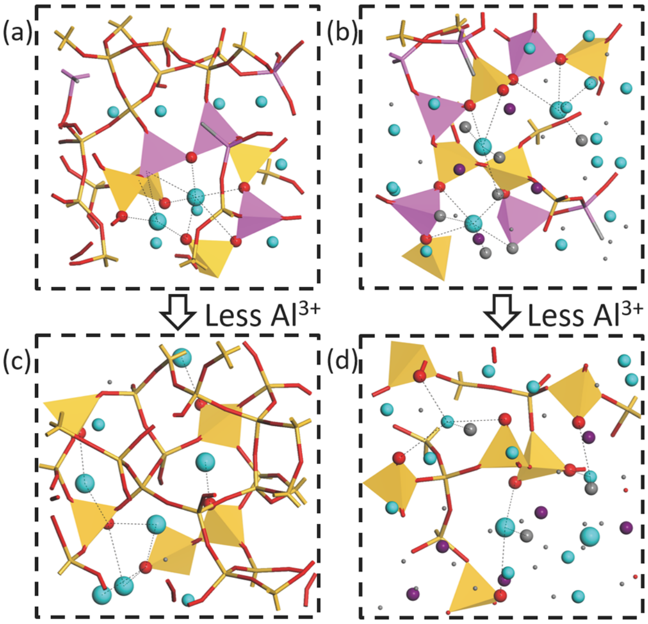

Figure 6. Na^+ coordination environment in the oxide phase (a) and phase interface (b) in G12Al and that in the oxide phase (c) and phase interface (d) in G0Al. Yellow: Si, pink: Al, purple: La, cyan: Na, grey: F, and red: O.

showing the mechanism of the Na^+'s preferential coordination with various Al/Si ratios. With a higher Al/Si ratio (Figure 6a,b), in the oxide network, Na^+ ions prefer to coordinate with $[AlO_4]$ through BO as charge compensators. After oxide network achieving electronic neutrality, the abundant Na^+ will therefore break the oxide network by coordinating with $[SiO_4]$, creating 1 NBO. On the two-phase interface, Na^+ have three ways to coordinate with the glass formers, the NBO from $[SiO_4]$ with Si−NBO−Na bonding, the BO from $[AlO_4]$ as the charge compensator with Al−BO−Na bonding, and the fluorine in $[AlO_xF_y]$ tetrahedra with Al−F−Na bonding. When Al^{3+} decrease (Figure 6c,d), Na^+ in both the oxide network and phase interface can only coordinate with $[SiO_4]$, creating 1 NBO. As observed in our earlier study,[37] Al^{3+} ions play an important role at the interface as it can bond to both oxygen and fluorine. Decreasing Al^{3+} in the glass composition will hence affect both the bulk and interfacial structures.

In addition, BAD shows that Na^+ prefers to coordinate with $[LaO_xF_y]$ and $[NaO_xF_y]$ polyhedral through fluorine bonding rather than with $[SiO_4]$ and $[AlO_xF_y]$ tetrahedra (Figure 7). The intensity of Na−F−Na and La−F−Na bonds is higher than other Na^+-related bondings and gets stronger with fewer

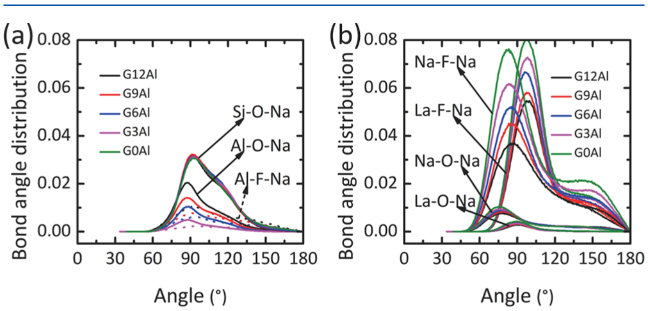

Figure 7. BAD of Na^+'s bonding with glass former tetrahedra (a) and modifier polyhedral (b) through oxygen and fluorine.

Al_2O_3. The unchanged in Si−O−Na bonding intensity shows the solubility limit of Na^+ in the oxide network. Coupled with the increase in F−Na−F bonding intensity, BAD confirms the preferential coordination of Na^+ in the fluoride phase with decreasing Al_2O_3 concentration.

4. DISCUSSION

4.1. Preferential Coordination of Na^+. With Al_2O_3 being substituted by SiO_2, Na^+ ion concentration decreases in the oxide phase and that increases in the fluoride phase. In this glass composition, Na^+ is the charge compensator for $[AlO_4]^-$ because of the appropriate size and charge state. When charge compensating $[AlO_4]^-$ tetrahedra, Na^+ coordinates with BO rather than creating NBO. When Al_2O_3 being substituted by SiO_2, the oxide network can maintain electronic neutrality with less Na^+. If Na^+ is still being in the oxide network, it will coordinate with $[SiO_4]$ tetrahedra, creating NBO, which will depolymerize the network. Consequently, the Na^+ staying in the oxide phase is not preferred. Besides, with the decrease of the Al/Si ratio, the oxide network will gradually become a silica-like glass (Figure 2d,e), whose solubility for Na^+ is poorer than the fluoride network. Therefore, with less Al^{3+} in the network, Na^+ prefers to coordinate in the fluoride phase to maintain the stability of glass samples.

4.2. Structural Origins of LaF_3, $NaLaF_4$, and NaF in Fluoride-Phase Separation. In this study, we observed representative clusters that are compositionally similar to the LaF_3, $NaLaF_4$, and NaF crystalline phases in fluoride-rich phase regions. It has been widely believed that phase separation is the initial stage of crystallization in the oxyfluoride glass system,[29,60] meaning that fluoride crystals are believed to precipitate from the fluoride phase or the oxide-fluoride phase interface. Here, with the decreasing Al/Si ratio, La−F, Na−F−La, and Na−F enrichment regions were found inside the fluoride phase (Figure 1). Correspondingly, from the experiment results,[45] LaF_3, $NaLaF_4$, and NaF precipitate, indicating that these specified enrichment regions can develop into different crystalline phases under certain conditions. Therefore, these enrichment regions can be viewed as the precursor for certain kinds of crystals.

4.3. Cubic to Hexagonal Phase Transition in $NaLaF_4$ Determined by Na^+ Concentration in the Separated Fluoride Phase. The cubic to hexagonal phase transition in $NaLaF_4$ nanocrystals is mainly determined by the Na^+ concentration in the fluoride phase. There are a number of experimental studies on oxyfluoride glass-ceramics with these crystals, but few of them discuss the phase transition. This is due to thermal treatment, rather than the composition adjustment, is most commonly used to obtain certain crystal phases in these glass ceramics. Here, as mentioned in Discussion part 1, the decrease of the Al^{3+} will cause the preferential coordination of Na^+ in the fluoride phase, making the precipitating $NaLaF_4$ crystalline phases transit from cubic to hexagonal, as suggested by the experiment results.[45] Similarly, Zhao et al.[36] studied oxyfluoride glass-ceramics with compositions $(60 + x)SiO_2-(18.5 - x)B_2O_3-9.5Na_2O-6NaF-6GdF_3$ (x = 0, 5, 10). It was also found that with less B_2O_3, the precipitate phase $NaGdF_4$ changes from cubic to hexagonal. Although they regard the reason for this phase transition to high viscosity and high internal pressure because of a higher SiO_2 concentration, the possibility of the decrease of B^{3+} leading Na^+ to decrease in the oxide phase and increase in the fluoride phase cannot be neglected. Adequate glass

DOI: 10.1021/acs.jpcb.9b01674
J. Phys. Chem. B 2019, 123, 3024−3032

modifiers will lead $[BO_3]$ transit to $[BO_4]^-$, requiring 1 Na^+ to charge compensate, which is similar to $[AlO_4]^-$ in this study. Therefore, by substituting B_2O_3 with SiO_2, Na^+ is not preferred by the oxide network in order to avoid depolymerization, being driven to the fluoride phase because of the higher solubility. Also, this higher Na^+ concentration in the fluoride phase induces the cubic $NaGdF_4$ to transit into the hexagonal crystalline phase. Beside, other paper in oxyfluoride glass systems also confirm the idea that a higher Na^+ ratio[28,61] in the glass composition or lower Al/Si ratio[8,20,45] favors the precipitation of hexagonal $NaRF_4$.

The higher concentration of Na^+ inducing the hexagonal $NaRF_4$ crystalline phase is also supported by the crystal precipitation from different media. The study by Thoma et al.[62] suggested that the formation of the cubic or hexagonal $NaRF_4$ phase does not only depend on the annealing temperature but also on the molar ratio of Na^+/R^{3+}. A larger Na^+ concentration results in the crystallization of the hexagonal phase, while a larger R^{3+} concentration favors the precipitation of the cubic phase. This effect was also described by papers[63,64] with the wet chemistry preparation of nanometer-sized $Na(Y,Gd)F_4$ crystals.

4.4. MD Simulations can Help To Predict Possible Crystalline Phase from Fluoride Phase Separation. Here, our MD simulation results provide insights into understanding the structure origins of crystalline phases and cubic to hexagonal phase transition from the experimental results, showing that MD simulation with effective potentials is a promising method to help to predict possible crystal phases from fluoride phase separation in aluminosilicate oxyfluoride glass. Many MD simulation studies in other glass systems, mostly oxide glass system, show its ability in understanding the glass structures and properties such as bioactivity,[65] mechanical properties,[59] surface interaction behavior,[53,66] electronic properties,[67] and so forth. However, very few studies focus on the crystallization behavior because of the limited time range that can be accessed through MD simulations that prevent direct simulation of nucleation and crystallization, except a few very simple systems. Thanks to the phase separation nature in the oxyfluoride phases, the relationship between the composition similarity of the fluoride-rich regions and crystal phases in oxyfluoride glasses can be established. By studying the fluoride phase separation, we can have a reasonable prediction of the possible crystalline phase that can be precipitated in the system. As a result, MD simulations can help in designing glass compositions with targeted crystal formation in oxyfluoride glass ceramics.

5. CONCLUSIONS

Classical MD simulations were used to investigate the composition-dependent fluoride phase separation in aluminosilicate glass. By using La^{3+} as model rare-earth ions R^{3+}, the structures of rare-earth ion-containing oxyfluoride aluminosilicate glasses with Al_2O_3/SiO_2 substitution were studied by using MD simulations. In the simulated glasses, phase separation was observed with the aluminosilicate-rich phase consisting of conventional $[SiO_4]$ and $[AlO_4]$ glass former units and the fluoride-rich phase consisting $[RO_xF_y]$ and $[NaO_xF_y]$ polyhedral. The results provide detailed structural information about both the short- and medium-range structure features on how the change of Al/Si affects the glass modifiers' enrichment in the fluoride phase. With a lower Al/Si ratio, Na^+ is more enriched in the fluoride phase while depleted in the aluminosilicate phase that led to an increase of polymerization of the network structures. The enrichment of Na^+ in the fluoride phase led to change of the abundance of linkages from R−F, to R−F−Na, and to Na−F, which can be considered as the structural origins of RF_3, $NaRF_4$, and NaF crystalline phase formation observed in experimental study, respectively. Furthermore, this higher Na^+ concentration in the fluoride phase is one of the main reasons for cubic to hexagonal phase transition in $NaRF_4$ crystals observed in different experiments. These structural details provide interpretations and insights into the experimental observed crystal phases in oxyfluoride glass ceramics. As a result, MD simulations can be an effective method to understand and explore possible crystal phases hence enabling computational-assisted design of oxyfluoride glass-ceramics.

■ ASSOCIATED CONTENT

Ⓢ Supporting Information

The Supporting Information is available free of charge on the ACS Publications website at DOI: 10.1021/acs.jpcb.9b01674.

Pair distribution function of Si−O and Si−F (a), Al−O and Al−F (b), Na−O and Na−F (c), La−O and La−F (d). Andcation−anion pair distance and cutoff distance (Å) used in bond angle distribution, coordination number, Q_n distribution, and ring size distribution analysis. (PDF)

■ AUTHOR INFORMATION

Corresponding Authors

*E-mail: qiaoxus@zju.edu.cn. Phone: +86-131-5716-9626 (X.Q.).

*E-mail: jincheng.du@unt.edu. Phone: +1-940-369-8184 (J.D.).

ORCID

Daqin Chen: 0000-0003-0088-2480

Xvsheng Qiao: 0000-0002-6411-1274

Jincheng Du: 0000-0003-4805-7498

Guodong Qian: 0000-0001-7133-2473

Xianping Fan: 0000-0003-4755-0934

Notes

The authors declare no competing financial interest.

■ ACKNOWLEDGMENTS

X.Q. acknowledges the funding from the National Nature Science Foundation of China (no. 51672243; 51872255). J.D. acknowledges US National Science Foundation DMR Ceramics Program (project # 1508001). J.Z. would like to thank Chinese Scholarship Council for the financial support when doing research in U.S.A. The computing services are provided by High Performance Computing facilities of University of North Texas, Denton, Texas USA.

■ REFERENCES

(1) Liu, X.; Zhou, J.; Zhou, S.; Yue, Y.; Qiu, J. Transparent Glass-Ceramics Functionalized by Dispersed Crystals. *Prog. Mater. Sci.* **2018**, *97*, 38−96.

(2) Fedorov, P. P.; Luginina, A. A.; Kuznetsov, S. V.; Osiko, V. V. Nanofluorides. *J. Fluor. Chem.* **2011**, *132*, 1012−1039.

(3) Kiprianov, A. A.; Karpukhina, N. G. Oxyhalide Silicate Glasses. *Glass Phys. Chem.* **2006**, *32*, 1−27.

(4) Gonçalves, M. C.; Santos, L. F.; Almeida, R. M. Rare-Earth-Doped Transparent Glass Ceramics. *C. R. Chim.* **2002**, *5*, 845−854.

(5) Dymshits, O.; Shepilov, M.; Zhilin, A. Transparent Glass-Ceramics for Optical Applications. *MRS Bull.* **2017**, *42*, 200−205.
(6) Chen, X.; Zhao, J.; Xu, X.; Ren, K.; Luo, X.; Sun, X.; Qiao, X.; Fan, X.; Qian, G.; Han, G. Phase Separation Strategy to Facilely Form Fluorescent [Ag2]2+/[Agm]n+ Quantum Clusters in Boro-Alumino-Silicate Multiphase Glasses. *Phys. Chem. Chem. Phys.* **2018**, *20*, 23942−23947.
(7) Wang, C.; Chen, X.; Luo, X.; Zhao, J.; Qiao, X.; Liu, Y.; Fan, X.; Qian, G.; Zhang, X.; Han, G. Stabilization of Divalent Eu2+ in Fluorosilicate Glass-Ceramics via Lattice Site Substitution. *RSC Adv.* **2018**, *8*, 34536−34542.
(8) Li, X.; Chen, D.; Huang, F.; Chang, G.; Zhao, J.; Qiao, X.; Xu, X.; Du, J.; Yin, M. Phase-Selective Nanocrystallization of NaLnF4 in Aluminosilicate Glass for Random Laser and 940 nm LED-Excitable Upconverted Luminescence. *Laser Photonics Rev.* **2018**, *12*, 1800030.
(9) Xu, X.; Zhang, W.; Yang, D.; Lu, W.; Qiu, J.; Yu, S. F. Phonon-Assisted Population Inversion in Lanthanide-Doped Upconversion Ba2LaF7 Nanocrystals in Glass-Ceramics. *Adv. Mater.* **2016**, *28*, 8045−8050.
(10) Cavillon, M.; Faugas, B.; Zhao, J.; Kucera, C.; Kukuoz, B.; Dragic, P.; Qiao, X.; Du, J.; Ballato, J. Investigation of The Structural Environment and Chemical Bonding of Fluorine in Yb-Doped Fluorosilicate Glass Optical Fibres. *J. Chem. Thermodyn.* **2019**, *128*, 119−126.
(11) Wang, C.; Wadhwa, A.; Cui, S.; Ma, R.; Qiao, X.; Fan, X.; Zhang, X. Dual Mode Temperature Sensing through Luminescence Lifetimes of F-and O-Coordinated Cr3+ Sites in Fluorosilicate Glass-Ceramics. *RSC Adv.* **2017**, *7*, 52435−52441.
(12) Wadhwa, A.; Wang, C.; Wang, C.; Ma, R.; Qiao, X.; Fan, X.; Qian, G. Multi-Phase Glass-Ceramics Containing CaF2:Er3+ and ZnAl2O4:Cr3+ Nanocrystals for Optical Temperature Sensing. *J. Am. Ceram. Soc.* **2019**, *102*, 2472−2481.
(13) de Pablos-Martín, A.; Durán, A.; Pascual, M. J. Nano-crystallisation in Oxyfluoride Systems: Mechanisms of Crystallisation and Photonic Properties. *Int. Mater. Rev.* **2012**, *57*, 165−186.
(14) Muñoz, F.; de Pablos-Martín, A.; Hémono, N.; Pascual, M. J.; Durán, A.; Delevoye, L.; Montagne, L. NMR Investigation of the Crystallization Mechanism of LaF3 and NaLaF4 Phases in Aluminosilicate Glasses. *J. Non-Cryst. Solids* **2011**, *357*, 1463−1468.
(15) Bhattacharyya, S.; Höche, T.; Hemono, N.; Pascual, M. J.; van Aken, P. A. Nano-Crystallization in LaF3-Na2O-Al2O3-SiO2 Glass. *J. Cryst. Growth* **2009**, *311*, 4350−4355.
(16) Środa, M.; Paluszkiewicz, C.; Reben, M.; Handke, B. Spectroscopic Study of Nanocrystallization of Oxyfluoride Glasses. *J. Mol. Struct.* **2005**, *744−747*, 647−651.
(17) Reben, M.; Wacławska, I.; Paluszkiewicz, C.; Środa, M. Thermal and Structural Studies of Nanocrystallization of Oxyfluoride Glasses. *J. Therm. Anal. Calorim.* **2007**, *88*, 285−289.
(18) Hémono, N.; Pierre, G.; Muñoz, F.; de Pablos-Martín, A.; Pascual, M. J.; Durán, A. Processing of Transparent Glass-Ceramics by Nanocrystallisation of LaF3. *J. Eur. Ceram. Soc.* **2009**, *29*, 2915−2920.
(19) Gu, Z.; Yan, L.; Tian, G.; Li, S.; Chai, Z.; Zhao, Y. Recent Advances in Design and Fabrication of Upconversion Nanoparticles and Their Safe Theranostic Applications. *Adv. Mater.* **2013**, *25*, 3758−3779.
(20) Sarakovskis, A.; Krieke, G. Upconversion Luminescence in Erbium Doped Transparent Oxyfluoride Glass Ceramics Containing Hexagonal NaYF4 Nanocrystals. *J. Eur. Ceram. Soc.* **2015**, *35*, 3665−3671.
(21) Wang, F.; Han, Y.; Lim, C. S.; Lu, Y.; Wang, J.; Xu, J.; Chen, H.; Zhang, C.; Hong, M.; Liu, X. Simultaneous Phase and Size Control of Upconversion Nanocrystals through Lanthanide Doping. *Nature* **2010**, *463*, 1061−1065.
(22) Krämer, K. W.; Biner, D.; Frei, G.; Güdel, H. U.; Hehlen, M. P.; Lüthi, S. R. Hexagonal Sodium Yttrium Fluoride Based Green and Blue Emitting Upconversion Phosphors. *Chem. Mater.* **2004**, *16*, 1244−1251.
(23) Mathews, M. D.; Ambekar, B. R.; Tyagi, A. K.; Köhler, J. High Temperature X-Ray Diffraction Studies on Sodium Yttrium Fluoride. *J. Alloys Compd.* **2004**, *377*, 162−166.
(24) Chen, D.; Wan, Z.; Zhou, Y.; Huang, P.; Zhong, J.; Ding, M.; Xiang, W.; Liang, X.; Ji, Z. Bulk Glass Ceramics Containing Yb3+/Er3+: β-NaGdF4 Nanocrystals: Phase-Separation-Controlled Crystallization, Optical Spectroscopy and Upconverted Temperature Sensing Behavior. *J. Alloys Compd.* **2015**, *638*, 21−28.
(25) Liu, F.; Ma, E.; Chen, D.; Yu, Y.; Wang, Y. Tunable Red-Green Upconversion Luminescence in Novel Transparent Glass Ceramics Containing Er: NaYF4 Nanocrystals. *J. Phys. Chem. B* **2006**, *110*, 20843−20846.
(26) Guo, Y.; Zeng, H.; Yang, B.; Chen, G.; Chen, J.; Sun, L. Gd3+ Doping Induced Enhanced Upconversion Luminescence in Er3+/Yb3+ Co-Doped Transparent Oxyfluoride Glass Ceramics Containing NaYF4 Nanocrystals. *Ceram. Int.* **2018**, *44*, 10055−10060.
(27) Zhao, S.; Sun, X.; Wang, X.; Huang, L.; Fei, Y.; Xu, S. The Influence of Phase Evolution on Optical Properties in Rare Earth Doped Glass Ceramics Containing NaYF4 Nanocrystals. *J. Eur. Ceram. Soc.* **2015**, *35*, 4225−4231.
(28) Herrmann, A.; Tylkowski, M.; Bocker, C.; Rüssel, C. Cubic and Hexagonal NaGdF4 Crystals Precipitated from an Aluminosilicate Glass: Preparation and Luminescence Properties. *Chem. Mater.* **2013**, *25*, 2878−2884.
(29) Lin, C.; Bocker, C.; Rüssel, C. Nanocrystallization in Oxyfluoride Glasses Controlled by Amorphous Phase Separation. *Nano Lett.* **2015**, *15*, 6764−6769.
(30) Bocker, C.; Wiemert, J.; Rüssel, C. The Formation of Strontium Fluoride Nano Crystals from a Phase Separated Silicate Glass. *J. Eur. Ceram. Soc.* **2013**, *33*, 1737−1745.
(31) Hill, R. G.; Goat, C.; Wood, D. Thermal Analysis of a SiO2-Al2O3-CaO-CaF2 Glass. *J. Am. Ceram. Soc.* **1992**, *75*, 778−785.
(32) Bocker, C.; Wiemert, J.; Rüssel, C. The Effect of Viscosity on Nanocrystallization of Strontium Fluoride from a Silicate Glass. *Solid State Sci.* **2014**, *30*, 55−60.
(33) Bocker, C.; Muñoz, F.; Durán, A.; Rüssel, C. Fluorine Sites in Glasses and Transparent Glass-Ceramics of the System Na2O/K2O/Al2O3/SiO2/BaF2. *J. Solid State Chem.* **2011**, *184*, 405−410.
(34) Bhattacharyya, S.; Höche, T.; Hahn, K.; van Aken, P. A. Various Transmission Electron Microscopic Techniques to Characterize Phase Separation−Illustrated Using a LaF3 Containing Aluminosilicate Glass. *J. Non-Cryst. Solids* **2009**, *355*, 393−396.
(35) de Pablos-Martín, A.; Pascual, M. J.; Durán, A. Transparent Nano-Glass-Ceramic for Photonic Applications-Distribution of RE-Doping Elements in the Fluoride Nano-Crystals Analysed by XAS and HR-TEM. *Advances in Science and Technology*, Trans Tech Publications, 2014; pp 111−120.
(36) Zhao, S.; Wang, X.; Sun, X.; Jia, G.; Huang, L.; Deng, D.; Xin, F.; Xu, S. Structural Evolution and Enhancement of Luminescence in the Eu-Doped Oxyfluoride Glass Ceramics Containing NaGdF4 Nanocrystals. *CrystEngComm* **2013**, *15*, 7346−7353.
(37) Zhao, J.; Ma, R.; Chen, X.; Kang, B.; Qiao, X.; Du, J.; Fan, X.; Ross, U.; Roiland, C.; Lotnyk, A.; Kienle, X. From Phase Separation to Nanocrystallization in Fluorosilicate Glasses: Structural Design of Highly Luminescent Glass-Ceramics. *J. Phys. Chem. C* **2016**, *120*, 17726−17732.
(38) Ali, M. A.; Ren, J.; Liu, X.; Qiao, X.; Qiu, J. Understanding Enhanced Upconversion Luminescence in Oxyfluoride Glass-Ceramics Based on Local Structure Characterizations and Molecular Dynamics Simulations. *J. Phys. Chem. C* **2017**, *121*, 15384−15391.
(39) Du, J. Challenges in Molecular Dynamics Simulations of Multicomponent Oxide Glasses. *Molecular Dynamics Simulations of Disordered Materials*; Springer, 2015; pp 157−180.
(40) Lusvardi, G.; Malavasi, G.; Cortada, M.; Menabue, L.; Menziani, M. C.; Pedone, A.; Segre, U. Elucidation of the Structural Role of Fluorine in Potentially Bioactive Glasses by Experimental and Computational Investigation. *J. Phys. Chem. B* **2008**, *112*, 12730−12739.

DOI: 10.1021/acs.jpcb.9b01674
J. Phys. Chem. B 2019, 123, 3024−3032

(41) Swansbury, L. A.; Mountjoy, G.; Chen, X.; Karpukhina, N.; Hill, R. Modeling the Onset of Phase Separation in CaO-SiO2-CaCl2 Chlorine-Containing Silicate Glasses. *J. Phys. Chem. B* **2017**, *121*, 5647−5653.

(42) Pedone, A.; Chen, X.; Hill, R. G.; Karpukhina, N. Molecular Dynamics Investigation of Halide-Containing Phospho-Silicate Bioactive Glasses. *J. Phys. Chem. B* **2018**, *122*, 2940−2948.

(43) Du, J.; Cormack, A. N. The Medium Range Structure of Sodium Silicate Glasses: A Molecular Dynamics Simulation. *J. Non-Cryst. Solids* **2004**, *349*, 66−79.

(44) Cormack, A. N.; Du, J.; Zeitler, T. R. Alkali Ion Migration Mechanisms in Silicate Glasses Probed by Molecular Dynamics Simulations. *Phys. Chem. Chem. Phys.* **2002**, *4*, 3193−3197.

(45) Peng, Y.; Zhong, J.; Li, X.; Chen, J.; Zhao, J.; Qiao, X.; Chen, D. Controllable Competitive Nanocrystallization of La3+-Based Fluorides in Aluminosilicate Glasses and Optical Spectroscopy. *J. Eur. Ceram. Soc.* **2019**, *39*, 1420−1427.

(46) Smith, W.; Forester, T. R. DL_POLY 2.0: A General-Purpose Parallel Molecular Dynamics Simulation Package. *J. Mol. Graphics* **1996**, *14*, 136−141.

(47) Xiang, Y.; Du, J.; Skinner, L. B.; Benmore, C. J.; Wren, A. W.; Boyd, D. J.; Towler, M. R. Structure and Diffusion of ZnO-SrO-CaO-Na2O-SiO2 Bioactive Glasses: A Combined High Energy X-Ray Diffraction and Molecular Dynamics Simulations Study. *RSC Adv.* **2013**, *3*, 5966−5978.

(48) Du, J.; Corrales, L. R. Compositional Dependence of the First Sharp Diffraction Peaks in Alkali Silicate Glasses: A Molecular Dynamics Study. *J. Non-Cryst. Solids* **2006**, *352*, 3255−3269.

(49) Ren, M.; Du, J. Structural Origin of the Thermal and Diffusion Behaviors of Lithium Aluminosilicate Crystal Polymorphs and Glasses. *J. Am. Ceram. Soc.* **2016**, *99*, 2823−2833.

(50) Xiang, Y.; Du, J.; Smedskjaer, M. M.; Mauro, J. C. Structure and Properties of Sodium Aluminosilicate Glasses from Molecular Dynamics Simulations. *J. Chem. Phys.* **2013**, *139*, 044507.

(51) Kokou, L.; Du, J. Short- and Medium-Range Structures Of Cerium Aluminophosphate Glasses: A Molecular Dynamics Study. *J. Non-Cryst. Solids* **2014**, *403*, 67−79.

(52) Deng, L.; Du, J. Effects of System Size and Cooling Rate on the Structure and Properties of Sodium Borosilicate Glasses from Molecular Dynamics Simulations. *J. Chem. Phys.* **2018**, *148*, 024504.

(53) Ren, M.; Deng, L.; Du, J. Surface Structures of Sodium Borosilicate Glasses from Molecular Dynamics Simulations. *J. Am. Ceram. Soc.* **2017**, *100*, 2516−2524.

(54) Greaves, G. N. EXAFS and the Structure of Glass. *J. Non-Cryst. Solids* **1985**, *71*, 203−217.

(55) Poulain, M. Glass Formation in Ionic Systems. *Nature* **1981**, *293*, 279.

(56) Xiang, Y.; Du, J. Effect of Strontium Substitution on the Structure of 45S5 Bioglasses. *Chem. Mater.* **2011**, *23*, 2703−2717.

(57) Stebbins, J. F.; Xu, Z. NMR Evidence for Excess Non-Bridging Oxygen in an Aluminosilicate Glass. *Nature* **1997**, *390*, 60−62.

(58) Lee, S. K.; Stebbins, J. F. The Structure of Aluminosilicate Glasses: High-Resolution 17O and 27Al MAS and 3QMAS NMR Study. *J. Phys. Chem. B* **2000**, *104*, 4091−4100.

(59) Du, J. Molecular Dynamics Simulations of the Structure and Properties of Low Silica Yttrium Aluminosilicate Glasses. *J. Am. Ceram. Soc.* **2009**, *92*, 87−95.

(60) Bocker, C.; Wiemert, J.; Rüssel, C. The Formation of Strontium Fluoride Nano Crystals from a Phase Separated Silicate Glass. *J. Eur. Ceram. Soc.* **2013**, *33*, 1737−1745.

(61) Cabral, A. A.; Balda, R.; Fernández, J.; Gorni, G.; Velázquez, J. J.; Pascual, L.; Durán, A.; Pascual, M. J. Phase Evolution of KLaF4 Nanocrystals and Their Effects on the Photoluminescence of Nd3+ Doped Transparent Oxyfluoride Glass-Ceramics. *CrystEngComm* **2018**, *20*, 5760−5771.

(62) Thoma, R. E.; Insley, H.; Hebert, G. M. The Sodium Fluoride-Lanthanide Trifluoride Systems. *Inorg. Chem.* **1966**, *5*, 1222−1229.

(63) Ptacek, P.; Schäfer, H.; Zerzouf, O.; Kömpe, K.; Haase, M. Crystal Phase Control of NaGdF4: Eu3+ Nanocrystals: Influence of the Fluoride Concentration and Molar Ratio between NaF and GdF3. *Cryst. Growth Des.* **2010**, *10*, 2434−2438.

(64) Ptacek, P.; Schäfer, H.; Kömpe, K.; Haase, M. Crystal Phase Control of Luminescing α-NaGdF4: Eu3+ and β-NaGdF4: Eu3+ Nanocrystals. *Adv. Funct. Mater.* **2007**, *17*, 3843−3848.

(65) Bonhomme, C.; Gervais, C.; Folliet, N.; Pourpoint, F.; Coelho Diogo, C.; Lao, J.; Jallot, E.; Lacroix, J.; Nedelec, J.-M.; Iuga, D.; Hanna, M. E.; Xiang, Y.; Du, J.; Laurencin, D. 87Sr Solid-State NMR as a Structurally Sensitive Tool for the Investigation of Materials: Antiosteoporotic Pharmaceuticals and Bioactive Glasses. *J. Am. Chem. Soc.* **2012**, *134*, 12611−12628.

(66) Du, J.; Xiang, Y. Investigating the Structure-Diffusion-Bioactivity Relationship of Strontium Containing Bioactive Glasses Using Molecular Dynamics Based Computer Simulations. *J. Non-Cryst. Solids* **2016**, *432*, 35−40.

(67) Du, J.; Corrales, L. R. Structure, Dynamics, and Electronic Properties of Lithium Disilicate Melt and Glass. *J. Chem. Phys.* **2006**, *125*, 114702.

DOI: 10.1021/acs.jpcb.9b01674
J. Phys. Chem. B 2019, 123, 3024−3032